ISTITUTO NAZIONALE DI FISICA NUCLEARE

Sezione di Milano

INFN/TC–98/03
2 Febbraio 1998

E. Bellotti, V. Bettinardi, I. Castiglioni, O. Cremonesi, F. Fazio, M.C. Gilardi, G. Rizzo, A. Savi, S. Schubert and C. Stearns:

3D POSITRON EMISSION TOMOGRAPHY: A MONTE CARLO STUDY OF SCATTERED RADIATION

PACS.: 87.70.e
Diagnostic Methods and Instrumentations

SIS–Pubblicazioni
dei Laboratori Nazionali di Frascati

Istituto Nazionale di Fisica Nucleare
Sezione di Milano

INFN/TC-98/03
2 Febbraio 1998

3D POSITRON EMISSION TOMOGRAPHY: A MONTE CARLO STUDY OF SCATTERED RADIATION

E. Bellotti[a], V. Bettinardi[b], I. Castiglioni[b], O. Cremonesi[a], F. Fazio[b], M.C. Gilardi[b], G. Rizzo[b], A. Savi[b], S. Schubert[c] and C. Stearns[c]

a Physics Department, Milan University, INFN Section, Milan, I-20123, Italy
b INB-CNR, Milan University, San Raffaele Institute, Milan, I-20132, Italy
c GE Medical Systems, Milwaukee, WI-53201, USA

A B S T R A C T

Developments in Positron Emission Tomography (PET) allow an increase in detection efficiency by a three-dimensional (3D) sampling of the radioactivity distribution in the source object. A drawback of this approach is related to the increased detection of scattered radiation, affecting the accuracy of PET images. Scatter correction techniques have to be used, which require knowledge of the spatial distribution of scattered radiation. In this study a Monte Carlo package (PET-EGS) was developed to simulate 3D PET scanners and radioactive sources. The package was modeled on the physical response of a 3D current generation PET scanner focussing on the study of scatter distribution. An analytical scatter correction technique, based on the assumption that scatter distribution can be described by a gaussian function, was evaluated through statistical analyses. Preliminary results indicate the validity of this approach with better accuracy for symmetrical radioactive sources. The feasibility of a probabilistic scatter correction method, based on the direct subctraction of Monte Carlo simulated scatter data from measured data, was also assessed, the results encouraging towards an extension of the method to clinical applications.

1. - INTRODUCTION

The detection of scattered radiations is one of the major sources of error in Positron Emission Tomography (PET), affecting both image quality and quantification accuracy [1]. This problem is particularly relevant in the recently developed three-dimensional (3D) PET technique, in which, due to the increased detection acceptance angle, the detected scatter component is higher with respect to that in the conventional bi-dimensional (2D) configuration [2-7]. Scattered radiations can be partially rejected during acquisition by use of discrimination energy windows. However, due to the poor energy resolution of PET detection systems (≈30%) [8-9], quite large energy windows are used (e.g. 300-650keV), reducing the efficacy of such electronic energy discrimination. The need for scatter correction techniques is thus well recognized [10-15]. Unfortunately, scattered radiations cannot be distinguished during acquisition from unscattered radiations and their spatial distribution, whose knowledge would be required for accurate scatter correction, cannot be experimentally determined.

Monte Carlo (MC) methods have been extensively used to simulate physical processes in PET in a large number of applications, such as the optimization of the detection system, the validation of reconstruction algorithms, the study of physical effects including radiation attenuation and scatter. In particular, as the MC method allows independent distributions of scattered and unscattered radiations to be obtained for known radioactive sources, it represents an useful tool to assess the feasibility and accuracy of scatter correction techniques [16-26].

In this work, a MC program was developed to simulate a current generation 3D PET tomograph. The program was modeled to simulate the Advance scanner (General Electric Medical Systems, Milwaukee, WI), installed in S.Raffaele Institute, Milan. Scatter distributions for simple geometric radioactive sources were studied by comparing experimental and simulated data. Finally, the MC program was used to evaluate different approaches (analytical and non-analytical) to scatter correction in 3D PET.

2. - PRINCIPLES OF POSITRON EMISSION TOMOGRAPHY

PET is a non-invasive diagnostic imaging technique producing images of radioactivity distribution in human body sections, following the administration of a radiopharmaceutical to the patient under examination. PET employes positron emitting radioisotopes, listed in Table 1 with their main physical characteristics. These radioisotopes have a short half-life, on the order of minutes, this implying the need for a cyclotron for their production in the proximity of the PET scanner. The costs related to such instrumentation and its complexity explain the limited diffusion of PET with respect to other imaging techniques. On the other hand, PET radioisotopes belong to biological elements, thus making physiological radioactive molecules available, whose kinetics can be assessed *in vivo* by external detection of the emitted radiations.

By measuring radioactivity concentration in the organ under study, PET allows metabolic functions and biochemical reactions to be quantitatively measured *in vivo*, this representing a unique feature of PET.

Radioisotope	Halftime (min)
^{18}F	109.8
^{11}C	20.4
^{13}N	10.0
^{15}O	2.0

Table 1

PET is based on the coincidence detection of the two 511keV γ radiations originating from the annihilation interaction of the positron, emitted from a radioactive nucleus in the body, with an electron of the sorrounding medium. A PET scanner consists of a number of adjacent rings of scintillator detectors (Bismuth Germanate, BGO, chosen for its high density and effective atomic number), connected by a temporal coincidence circuitry. Radioactivity in the body is thus sampled at different linear and angular positions and these radioactivity projection data are then processed by reconstruction mathematical algorithms to generate images of radioactivity distribution [27].

PET has been originally developed as a bi-dimensional (2D) technique, with inter-plane septa, positioned in between two adjacent rings to avoid the detection of oblique radiations and in particular of scattered radiations. A set of 2D transaxial images is then obtained, each image being generated by the detection of coincidence events between detectors within the same ring (direct plane) or in adjacent rings (cross plane). More recently a 3D approach to the PET technique has been developed. By removing the inter-plane septa, the axial acceptance angle can be increased, allowing the detection of all possible coincidences. This results in a significant increase in the number of detected events, although scattered radiations, originated from Compton interactions in the radioactive source, largely contribute to this increased sensitivity (scatter component on the order of 30-40%) [28-33]. In order to accurately quantify radioactivity concentration, the use of scatter correction techniques is compulsory.

Advantages of the increased sensitivity provided by the 3D approach (by a factor of ≈6, accounting for scatter component) are found both in clinical and research applications, allowing either an improvement in image quality in terms of signal/noise ratio or a reduction of the radiation dose administered to the patients [34-38]. The 3D PET approach has proved very important when repeated PET measurements are desired, as in PET activation studies [39] and

particularly in low count rate studies (e.g. paediatric studies, receptor studies) [40]. Fig.1 shows some representative images for a PET study with ^{18}F -Fluoroethylspiperone ([^{18}F]FESP), performed in 2D mode (top) and 3D mode (bottom). ^{18}F-Fluoroethylspiperone is a tracer of the D2 dopaminergic and of the S2 serotoninergic receptors. To note, the improved image quality and signal/noise ratio in 3D images.

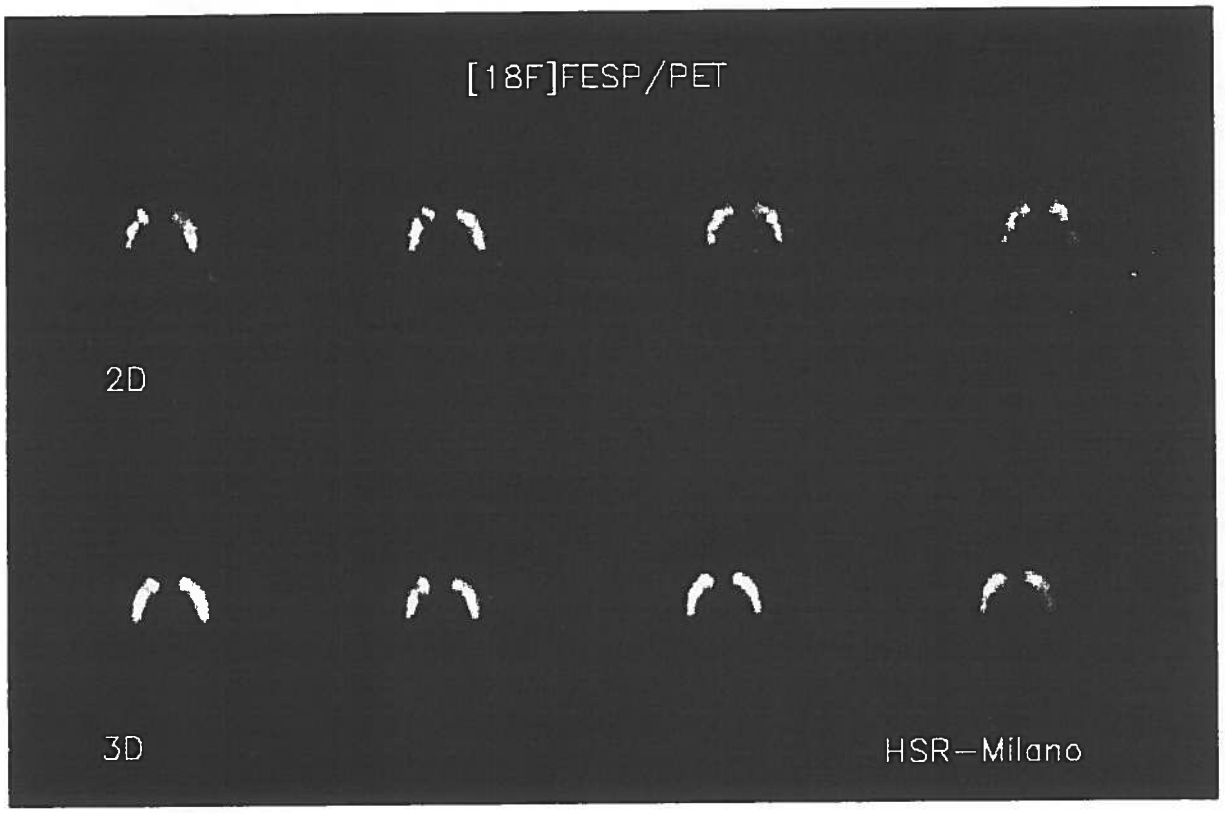

Fig. 1
[^{18}F]FESP study in 2D mode (top) and in 3D mode (bottom)

3. - 3D PET CURRENT GENERATION SCANNER ADVANCE

The Advance PET scanner consists of 18 rings (92.7cm diameter) of 672 BGO crystals (4x8.1x30mm^3 each), covering an axial field of view (FOV) of 15.2cm. The detection unit is a block of 6x6 crystals, coupled to two dual photomultipliers (PMTs). Identification of the crystal where a photon has interacted in a block is obtained by weighting block PMT signals in a way similar to the Anger gamma-camera signal analysis technique [41]. Energy lost in a block is determined by the sum of the PMT signals. Energy resolution for a detection block has been reported to be ≈33% [9]. An energy window (300-650 keV) is set to reject part of scattered radiations.

Each crystal is in coincidence with 283 opposite crystals (transaxial acceptance angle: 75°), yielding a transaxial FOV of 55cm. The time coincidence window is 12.5ns wide.

Coincidence events are organized in sinogram matrices (one sinogram per acquisition plane), whose size is 336x283, 336 being the number of angular projections and 283 being the number of linear samplings at each angle.

The scanner is equipped with external tungsten rings to shield from radiations generated outside the scanner FOV. In 2D mode inter-plane septa physically separate detector rings. Coincidence events between detectors within the same ring and in adjacent rings are accepted, generating direct and cross planes respectively. Thirty-five image planes (18 direct and 17 cross planes) are thus yielded. In 3D mode, inter-plane septa are automatically retracted and all possible coincidences are recorded in 18x18=324 acquisition planes, which are processed by a 3D reconstruction algorithm to generate 35 image planes (according to the 2D image configuration) [42-43].

4. - MONTE CARLO SIMULATION OF A 3D PET SCANNER

4.1. - PET-EGS MC software package

A MC software package was developed to simulate current generation 3D PET scanners and geometrical radioactive sources. The package is based on the EGS4 code [44] and is developed under a criterion of versatility to guarantee: a) the possibility of simulating a variety of multiple ring 3D PET tomographs and radioactive sources and b) the possibility of a flexible analysis of the simulated data, allowing different information to be extracted from the same data set.

According to this parametric approach, the package consists of a main program (PET-EGS), interfacing with the user through input and output files and with the EGS4 code through calls to libraries, which calculate cross-section data and simulate different radiation interaction processes. Both main program and libraries are written in C and Fortran languages and run under Unix operating system on SUN Sparc or HP workstations.

The main program outlines the three-dimensional space physical regions, simulates radiation histories through the different regions using a random number generator to account for stochastic variables (e.g. position of the radiation emission point, flight direction, interaction probability), geometrically calculates the intersections between radiation paths and physical regions.

The configuration of the experimental set up under simulation is defined by the user in the input file, by simply setting the inherent parameters (e.g. shape, size and material for both the detection system and the radioactive source). The number of radioactive events to be simulated is also set in the input file. The output files contain energy and spatial information relative to each photon interaction. The information to be stored in the output files are selected by the user in the input file.

4.2. - Scattering and attenuating media

Physical regions, describing the 3D space, include the radioactive source, the inter-space between the source and the detection system, the detectors, the edge shields, the outside space (Fig.2).

Each region is described analytically by a geometrical function in the 3D space and is associated to a medium of known composition.

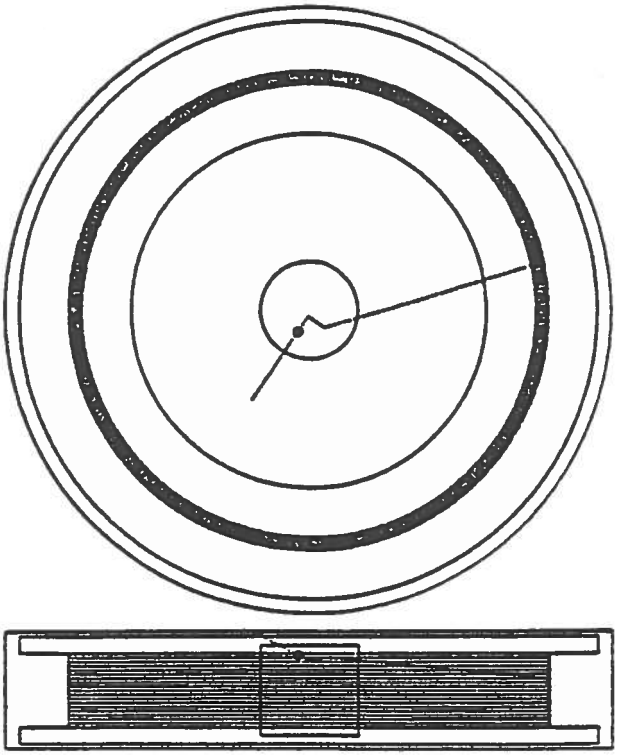

Fig. 2
Geometrical set up of a current generation 3D PET scanner:
the transaxial (above) and the axial (bottom) perspective.
In this case a scattered event is occurred in a uniform 20cm cylindrical source.

4.3. - Radioactive sources and photon histories

Radioactive sources are positron emitters. Positron histories (thus positron ranges) are neglected during simulations and the assumption is made that the positron emission point is coincident with the γ rays annihilation point. A radioactive event is simulated as the emission of a pair of anti-parallel annihilation γ rays. The annihilation point in the source region and the

flight direction for the first of the two annihilation 511keV γ rays (γ1) are random generated. The second annihilation photon (γ2) is generated in the same emission position, but with anti-parallel flight direction with respect to γ1. Effect of non-collinearity (deviations from the original flight direction) is not considered during simulation. Both the range and the non-collinearity effects are accounted for by analytical models after simulation (see below, "Data sorting after simulation").

Histories of γ rays are simulated according to the EGS4 code by randomly generating the point of interaction within the current region and randomly sampling Rayleigh, Compton and photoelectric absorption cross-sections (σ_R, σ_C, τ_P), the probability for any interaction to occurr being then given by $\mu = \sigma_R + \sigma_C + \tau_P$ [45]. In Compton scattering, the angular distribution of scattered γ rays is predicted by the Klein-Nishina formula for the differential scattering cross-section [465], having generated a random diffusion angle. The energy of the scattered photon is calculated and its history is tracked. In photoelectric event, the photoelectron propagation and the characteristic X radiations (with low energy with respect to 511keV in the considered media) are not simulated, beacuse not involved in the PET detection process.

4.4. - 3D PET detection system

A 3D PET scanner is simulated as a number of detection rings, each ring consisting of a number of scintillator crystals. Crystals are simulated as adjacent in the transaxial plane and in the axial direction. Inter-ring/inter-crystal gaps are filled by scintillator material. Two external shields are simulated as heavy material rings located at the two axial edges of the tomograph.

The detection block, typical of current generation PET scanners, is simulated by grouping crystals in matrices. Photon history within a crystal, across crystals within a block and across blocks is tracked. The detection of a photon within a block is associated to the crystal in which the highest fraction of energy was lost by the photon. The transport of light produced during scintillations in the crystals is not simulated nor the block associated electronic chain (PMTs, pre-amplifiers and amplifiers). Degradation of spatial resolution due to in-block scatter and position decoding error (block blurring effect) and degradation of energy resolution due to light distribution in the block and to electronic components are analytically modeled after simulation (see below, "Data sorting after simulation") [19].

A coincidence event is recognized when both the annihilation photons are detected. As the MC program does not include temporal information, random coincidences are not simulated. Coincidences are classified as "scattered" or "true" depending on whether or not one or both photons have Compton scattered in the source object.

The history of two annihilation 511keV γ rays is graphically shown in Fig.2 in a representative case.

4.5. - Data sorting after simulation

Spatial and energy parameters, stored on an event-by-event basis in the output files during simulation, are *a posteriori* processed and re-organized by dedicated data analysis programs to produce global information on the simulated radioactive source and the simulated 3D PET scanner.

Energy resolution and energy spectra

Energy data can be sorted in energy spectra, describing the distribution of energy lost by photons in the source object and in the detection system. Energy spectra relative to various components of the detection system can be created (e.g. whole blocks or individual crystals), this feature representing an useful tool in the use of the MC program for the assessment of the performance of the detection system and in the optimization of its design.

The effect of the limited energy resolution of the detection system (which was not accounted for during simulation) is modeled by spreading the values of the energy lost by the photons at each interaction by a gaussian function with a width equal to the energy resolution of the detection system.

Sinogram creation and intrinsic spatial resolution

Spatial data can be sorted in sinogram matrices. Each sinogram element is associated to a pair of crystals in coincidence, through a sorting algorithm, which is specific to each PET scanner. Each sinogram element contains the number of coincidence events detected by the associated pair of crystals.

Energy discrimination is performed during sinogram creation. A coincidence event is accepted to contribute to the sinogram when the energy lost by both the annihilation photons in the blocks falls within the discrimination energy window. Energy thresholds are selected by the user.

Combining spatial and energy information, coincidence events for which one or both photons have scattered in the source object can be separated to create independent scatter sinogram data.

A sinogram post-processing program accounts for physical phenomena affecting system intrinsic spatial resolution and not considered during simulation. Sinograms are processed line by line (each line representing an angular projection profile) by convolution with a gaussian function with appropriate width (σ) [19]:

$$\sigma_{gauss}^{2} = \sigma_{range}^{2} + \sigma_{non\text{-}col}^{2} + \sigma_{block}^{2} \qquad (1)$$

where

σ_{range} accounts for the loss of resolution due the positron range;

$\sigma_{non\text{-}col}$ accounts for the loss of resolution due to the annhilation photon non-collinearity effect. This value is estimated in the centre, where this effect is maximum, and assumed constant over the whole FOV;

σ_{block} accounts for the loss of resolution due to the block blurring effect.

5. - MODELING PET-EGS PACKAGE TO THE ADVANCE 3D PET SCANNER

The Advance PET scanner was simulated by the PET-EGS package, by setting in the input file the physical characteristics of the detection system as described in Section 3. Experimental measurements of a line source in air and in scattering medium were performed and the same conditions were reproduced by MC simulation. Comparison of measured and simulated physical parameters (intrinsic spatial resolution and scatter fraction) allowed the MC simulator to be modeled to the physical response of the Advance scanner and the validity of modeling to be verified.

5.1. - Intrinsic spatial resolution

Materials and Methods

A radioactive linear source of ^{18}F, encapsulated in a steel needle (30cm long, 1.1mm inner diameter, 1.6mm external diameter) was placed in air parallel to the axis of the tomograph at 0, 10, 20cm off centre. 3D PET measurements were performed collecting 20-30 million counts per study. The same measurements were simulated by generating 10 million photon pairs per study.

Measured and simulated sinograms relative to the 35 detection planes corresponding to the 2D acquisition configuration were extracted from the whole 3D data set. Profiles of radioactivity distribution were generated by averaging over the 336 angular views to improve signal/noise ratio (applying proper spatial shift when the radioactive source was off centre, in order to have all profile peaks aligned in the centre). Simulated profiles were convolved with a gaussian function with appropriate width (σ_{gauss}) to account for physical phoenomena affecting spatial resolution and not included in simulation (see Section 4). The following contributions to σ_{gauss} were considered for the Advance scanner [46]:

σ_{range} = 1mm for ^{18}F. The effect of positron range could be neglected in this specific situation, as positrons were completely absorbed in the steel needle wall (σ_{range}=0);

σ_{uncol} = 2.4mm in the centre of the field of view;

σ_{block} = 2mm

According to equation (1), the resulting width of the gaussian function was then:

$$\sigma_{gauss} = \sqrt{(2.4^2 + 2^2)}\ \text{mm} = 3.12\text{mm}$$

Intrinsic spatial resolution was defined by the Full Width Half Maximum (FWHM) and Full Width Tenth Maximum (FWTM) of the spatial distribution profiles. Measured - simulated values were compared.

Results

Profiles of radioactivity distribution from a representative sinogram for the line source at 1, 10, 20cm off centre are shown in Fig.3. Note the good agreement between measured and simulated distributions for all source positions.

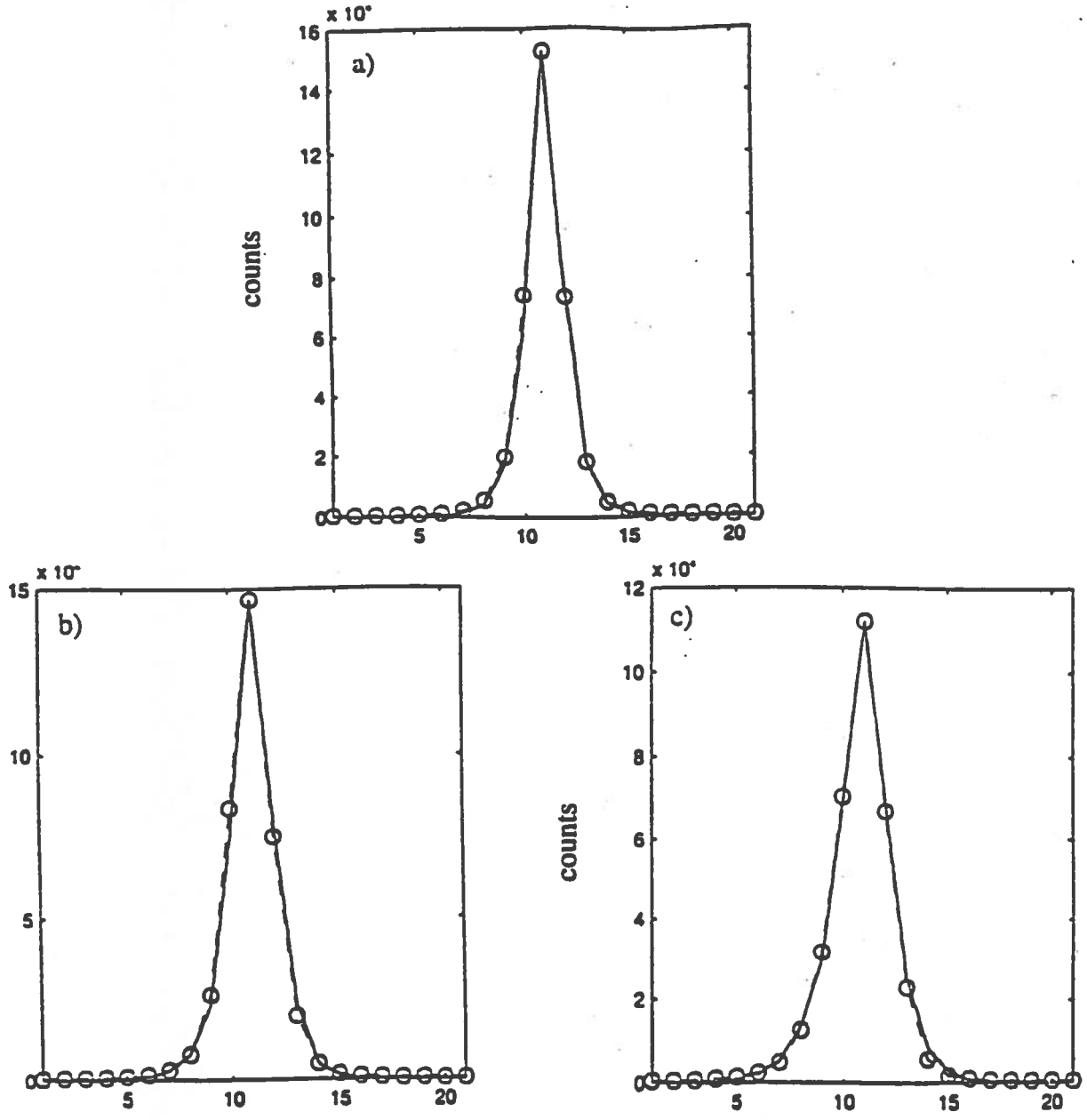

Fig. 3

Measured (o) and simulated (-) radioactivity profiles

for a line source at 1cm (a), 10cm (b), 20cm(c) off center

Values of intrinsic spatial resolution (FWHM, FWTM), averaged over the 35 planes, are summarized in Table 2 and graphically presented in Fig.4, as a function of the source distance from centre. Spatial resolution does not change significantly over the 35 planes (standard error within 4%).

offset (cm)	measured FWHM (mm)	simulated FWHM (mm)	% difference	measured FWTM (mm)	simulated FWTM (mm)	% difference
1	4.57	4.35	4.83	9.97	9.56	4.14
10	4.84	4.67	3.45	10.45	10.20	2.39
20	5.41	5.26	2.77	11.52	11.52	0

Table 2

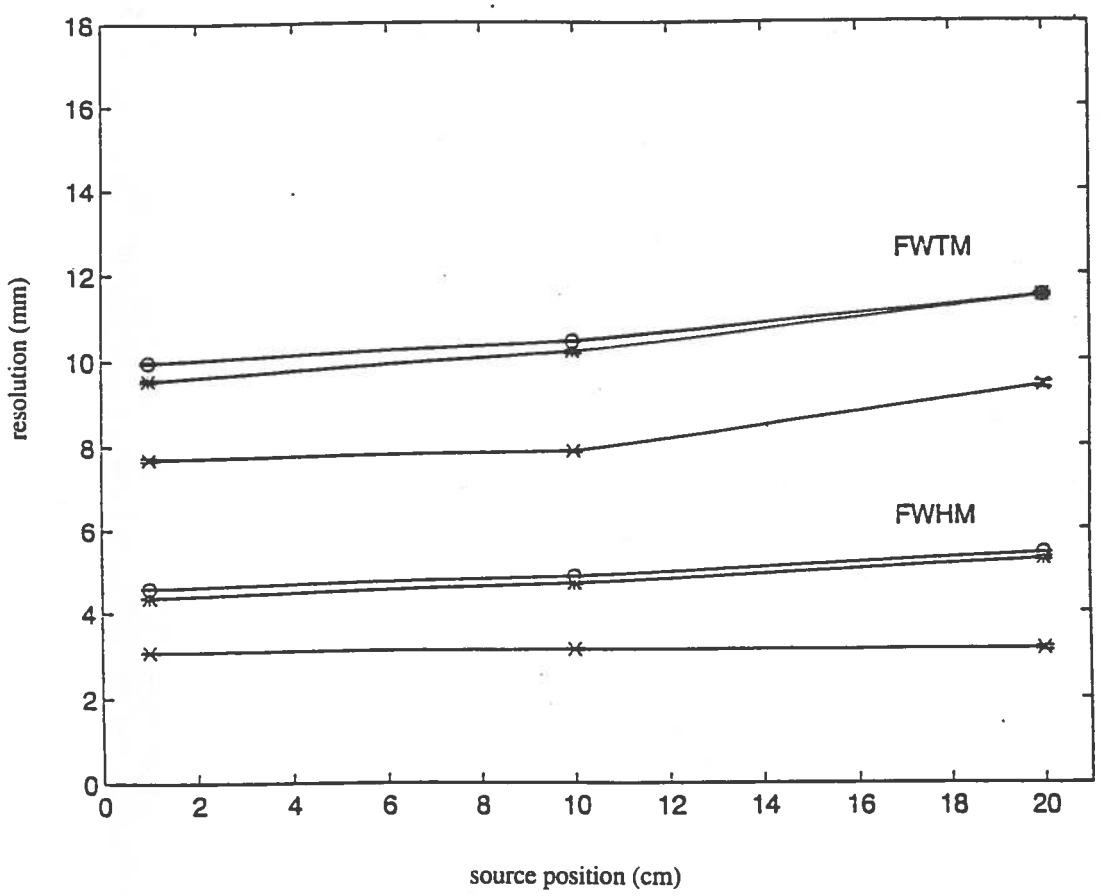

Fig. 4

Measured (o), simulated (x) and convolved simulated (*) intrinsic resolution as a function of the source position (cm).

In-plane spatial resolution increases towards the edge of the field of view. This effect is explained by the angled position of the detectors with respect to an off-centre radioactive source, resulting in a higher probability of crosstalk between adjacent detectors [41].

Convolution properly accounts for non simulated physical effects (positron range, non-collinearity effect, block blurring) and percent differences between measured and convolved simulated resolution values are within 5%. An apparent better agreement at the edge of the FOV was observed, which can be attributed to the off-centre overestimation of the non-collinearity component in the convolved simulated data.

As a result of this analysis, the effect of spatial resolution can be reproduced by convolving the profiles of the simulated sinograms with gaussian functions, whose width is defined by equation (1). However, in following analyses, in order to reproduce the effective spatial resolution of the Advance scanner, an additional quadratic term was introduced in equation (1) to account for the residual difference between measured and simulated values.

5.2. - Scatter Fraction

Materials and Methods

A radioactive linear source of ^{18}F, encapsulated in a glass needle (18.5cm long, 1.1mm inner diameter, 1.6mm external diameter) was placed within a 20cm diameter water cylindrical phantom, parallel to the axis of the tomograph at 0, 4, 8cm off centre. 3D PET measurements were performed collecting 40-50 millions counts per study. The same measurements were simulated by generating 20 million photon pairs per study.

A representative sinogram profile obtained by averaging over the 35 planes and over the 336 angular views (applying proper spatial shift for off centre sources) was generated for both measured and simulated data. Simulated profiles were convolved with gaussian functions, to account for the effective system spatial resolution, as defined above.

Scatter fraction was defined for each source position according to standard procedures [47] as the ratio of scattered events to total events (true coincidences + scatter coincidences). Total events were calculated as the integral of counts under the sinogram profile. Scattered events were determined as the integral of the sinogram profile, assuming a constant background under the peak, the level of which was calculated as the average of counts at the edge of the peak (± 2cm from peak maximum). Scatter fraction (SF) for the whole phantom was determined as the mean of the scatter fraction values estimated at each source position (SF_0, SF_4, SF_8), weighted by the area of the annulus at that radius:

$$SF = (SF_0 + 8 \cdot SF_4 + 16 \cdot SF_8)/25 \qquad (2)$$

Results

Values of scatter fraction (measured and simulated) at 0, 4, 8cm off centre and for the whole phantom are reported in Table 3.

	offset (cm)	measured scatter fraction (%)	simulated scatter fraction (%)	% difference
line source	0	41.9	37.7	10.0
	4	41.5	39.9	3.8
	8	36.8	33.9	7.3
uniform cylinder	0	38.5	36.0	6.4

Table 3

Simulated scatter fraction was underestimated with respect to measured values within 10%. For the whole phantom, difference was 6.4%. Such underestimation can be explained by radiations scattered in the surrounding environment (wall, scanner bed, etc.), which are not accounted for during simulation.

The good agreement between exprimental and simulated data proves that, given the assumptions made in the MC model, the response of the PET scanner is accurately reproduced by simulation.

6. - MC STUDY OF SCATTERED RADIATION IN 3D PET

The use of the Monte Carlo program was focussed to the study of scattered radiations in 3D PET. This application takes advantage of the capability of the MC method to separate true coincidences from events scattered in the source object. Topics inherent to the scatter issue were addressed as described below.

6.1. - MC investigation of 3D scattered radiation

MC investigation of the distribution of scattered radiations in 3D PET represents a necessary preliminary step to the implementation and evaluation of scatter correction techniques. The MC program was used to simulate scatter distribution in the case of simple geometric radioactive sources.

Materials and Methods

Two cylindrical sources filled with a uniform solution of water and ^{18}F were studied (cylinder A: D=20cm, L=18.5cm; cylinder B: D=7.8cm, L=25.8cm). 3D PET measurements were performed collecting 500 and 250 million counts per study for cylinder A and B respectively. MC simulations were obtained generating 200 and 20 million counts for cylinder A and B respectively.

Data from the line source in water (at 0, 4, 8cm off centre) measured and simulated for the study of scatter fraction (see paragraph 5 above) were also considered.

For all MC simulated sources, scattered events were separated from true events, thus creating independent sinograms. Measured and scatter simulated sinograms relative to the 2D 35 detection planes were extracted from 3D data. Profiles of radioactivity distribution were generated by averaging over the 35 planes and the 336 angular views (applying proper spatial shift when the radioactive source was off centre).

Results

Average profiles of radioactivity distribution for all sources considered are shown in Fig.5. Simulated profiles of scatter distribution are shown, after normalization, overlapped to measured profiles (including both scatter and true events). Spatial distribution is well described by the simulations for all the sources in terms of shape and amplitude of scatter component. Note in paricular the good agreement between simulated and measured profiles outside the object source. In fact, scatter region covers the whole FOV, extending outside the scattering medium without discontinuity in correspondence of the object edges.

A non-symmetrical shape of scatter component in the profiles relative to non-symmetrical sources is observed, reflecting the dependence of scatter component on the radioactivity distribution in the source (Fig.5d,e). However, the shape of the profile in the region underlying the radioactive source appears quite smooth. This loss of spatial information can be explained by the wide energy window used (300-650keV) resulting in a large contribution of detected events scattered at large angles [16,48]. Such a flat distribution of 3D scattered events supports the possibility of modeling scatter distribution by low frequency analytical functions, this approach representing the background for various scatter correction methods employed in 3D PET [13,50].

6.2. - MC evaluation of a gaussian fitting scatter correction method

The scatter correction method implemented on the Advance PET scanner is based on the assumption that the scatter distribution is a low frequency function and relatively insensitive to the activity distribution. The method consists in processing each angular profile in the sinograms, as follows: 1. modeling the scatter component by fitting a gaussian function to the tails of the measured radioactivity profiles, outside the source object, 2. extrapolating the fittting inside the object and 3. subtracting such estimated scatter distribution from the measured profiles [5,49]. Although the method is simple and fast, this explaining its wide diffusion, the accuracy of a gaussian modeling of the scatter distribution should be verified. This task can be accomplished by use of MC simulations, generating the scatter component for any radioactive source over the whole FOV of the tomograph. A characteristic low frequency behaviour of scatter component was observed in the study of scatter distribution in the case of cylindrical and line sources (see Section 6.1).

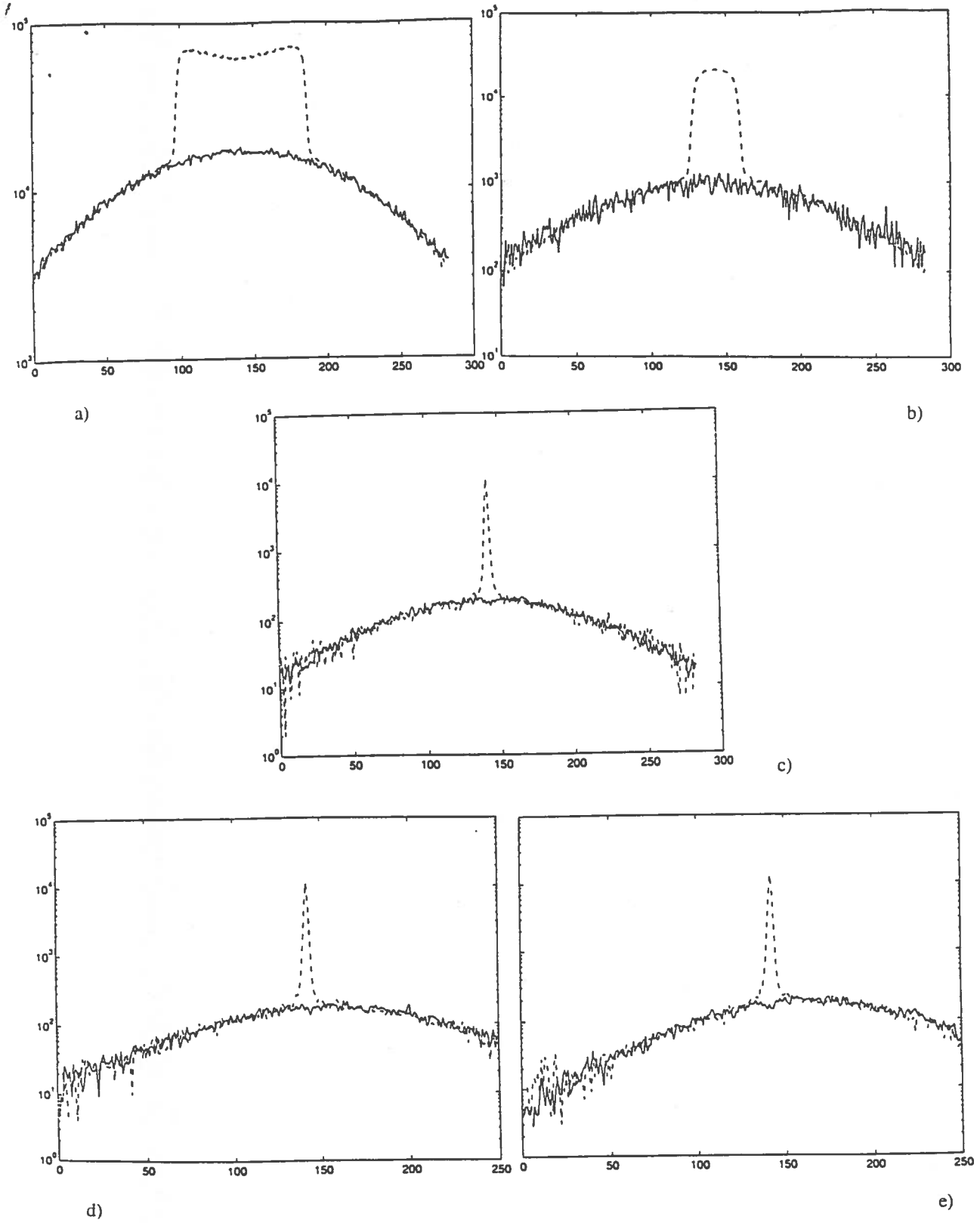

Fig. 5

Trues + Scatter Measured (--) and scatter simulated (-) radioactivity profiles for all the considered source: the 20cm uniform cylinder (a), the 8cm uniform cylinder (b), the line source in the 20cm water cylinder at 0cm (c), 4cm (d), 8cm (e) off center.

Aim of this study was to evaluate the accuracy in modeling the distribution of scattered events by a gaussian function.

Materials and methods

A gaussian fitting was applied to data generated by MC simulations in the case of high counting statistics simulations relative to the symmetrical 20cm cylinder (200 million counts) and to the non-symmetrical line source in water at 8cm off axis (extending simulation up to 70 million counts). High counting statistics data were necessary, as scatter correction acts on single angular profiles and averaging could thus be performed only in the axial direction over the 35 planes. To further improve signal/noise ratio in each angular profile, data were averaged every four pixels, thus obtaining 71 sampling points for each profile. For both simulated sources, each angular profile was iteratively fitted to a gaussian function by minimizing the χ^2 value.

Results

Simulated profiles and the fitted gaussian functions are shown overlapped in Fig.6 for both the 20cm cylinder and the line source at two selected angles.

As expected, the 20cm cylindrical source shows similar profiles at any angle, while the 8cm off-centre line source is characterized by angular profiles changing in shape according to the shift of the position of the source at the various angles.

The distribution of χ^2 values over the 336 angular profiles are presented in Fig.7 in histogram form.

Simulated average values and expected values for χ^2 and for $\sqrt{\chi^2}$ are reported in Table 4 for the symmetrical source (the 20cm cylinder) and for the asymmetrical source (the 8cm off centered line source).

For both sources, average and expected values were in agreement within one σ value, proving that gaussian function well modeled scatter distribution. Better accuracy was found in the case of the symmetrical source.

	χ^2	$\sqrt{\chi^2}$
expected value	67.5	11.6
simulated average value for the symmetrical source	66	11.1
simulated average value for the asymmetrical source	74	12

Table 4

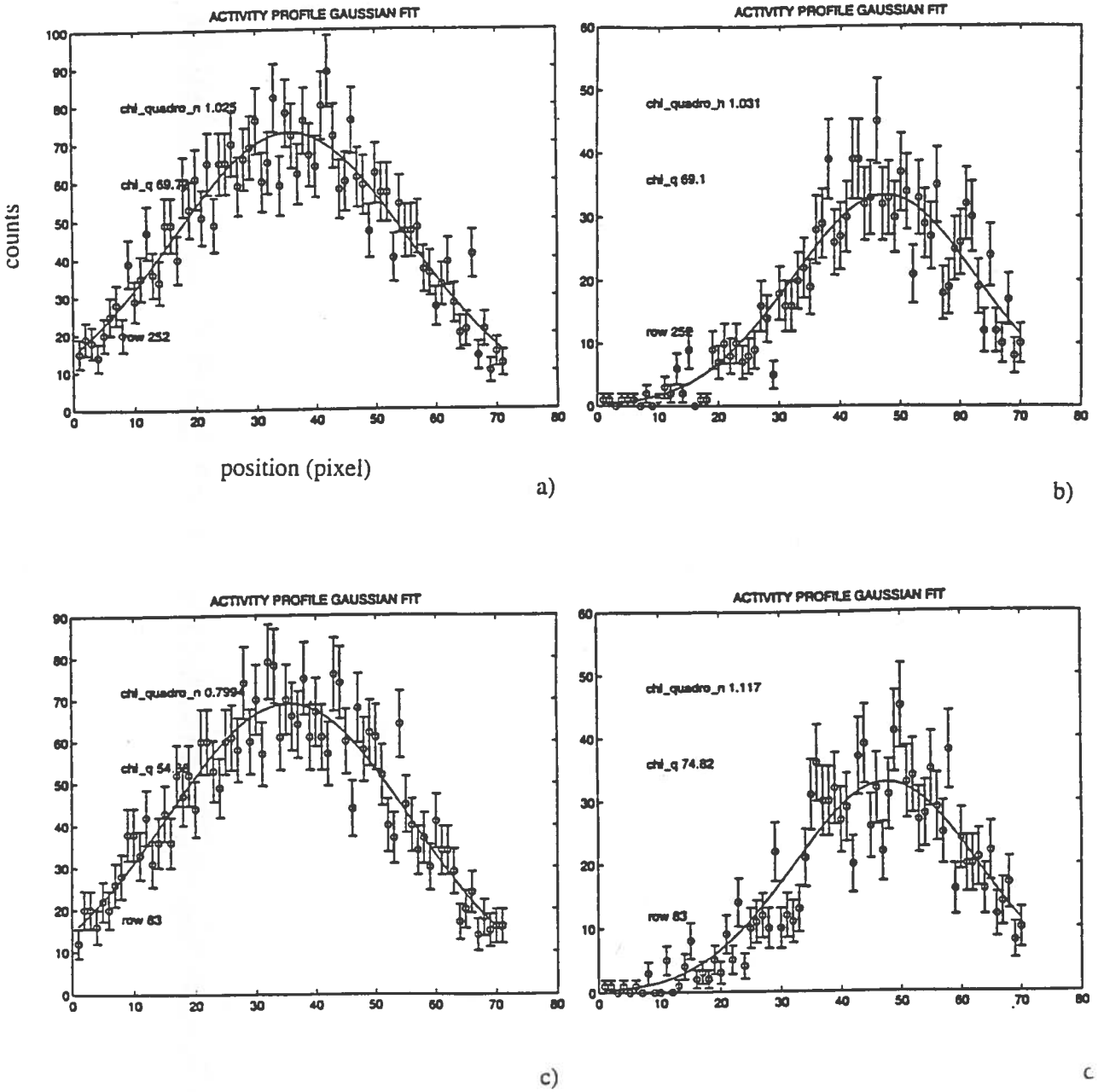

Fig. 6

Gaussian fits of two angular scatter spatial profiles :
for the symmetrical source at 135° (a) and at 45° (c)
and for the asymmetrical source at 135° (b) and at 45° (d).

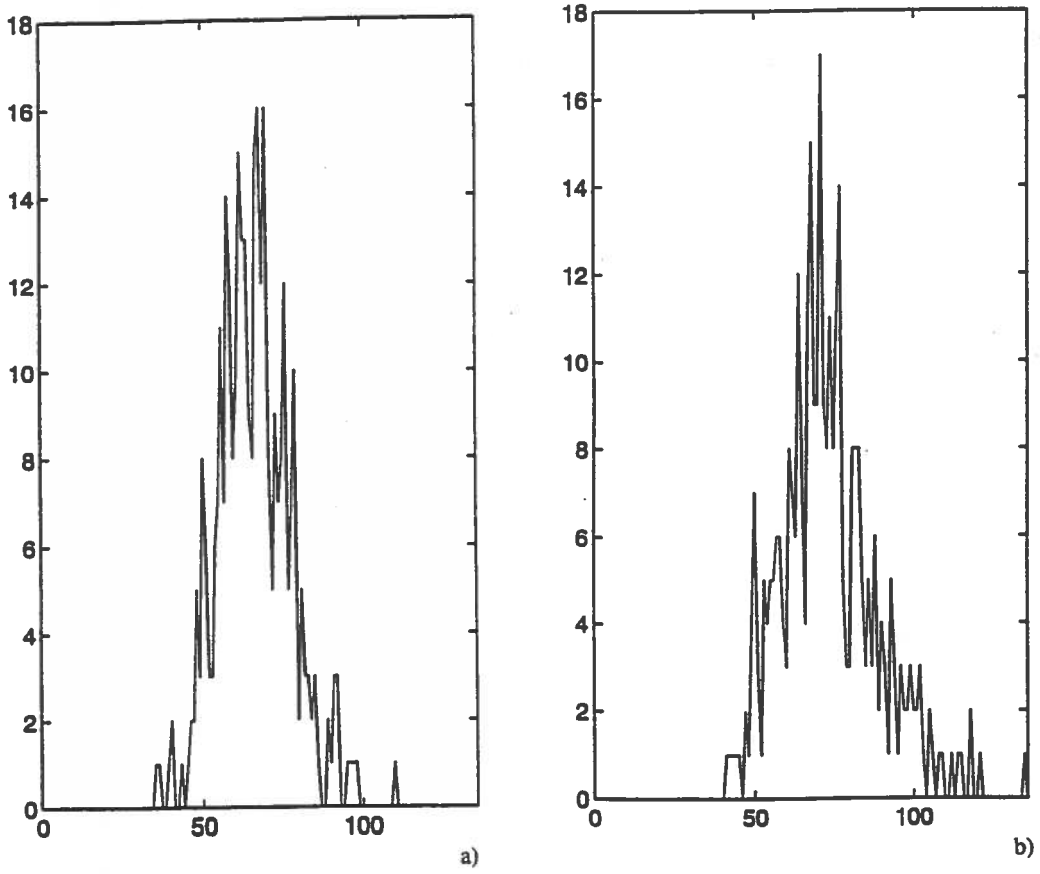

Fig. 7

χ^2 distribution for the symmetrical source a) and the asymmetrical source b)

6.3. - MC scatter correction method

An alternative approach to scatter correction was proposed by Levin et al. [50], based on the MC simulation of the scatter distribution in the source object. The method uses the reconstructed 3D PET images as known radioactivity distribution in the source object. Scatter component is MC simulated and subtracted from measured data. The advantage of this approach is that it does not make assumptions on scatter distribution, but accounts for the real distribution of radioactivity and scattering/attenuating media present in the source object. A limitation of this approach is however that 3D PET images used as sources in MC simulations contain a considerable amount of scattered events, erroneously interpreted by the MC method as real radioactivity in the source, thus limiting the accuracy of a MC based scatter model.

Aim of this study was to use the implemented MC simulation package to develop the scatter correction method proposed by Levin et al. [50], assuming, at this stage, scatter-free synthetic geometrical objects as true radioactivity source distributions.

Materials and methods

Measued and scatter simulated data used in the MC study of scatter distribution were considered (two cylindrical sources and three line sources in water, Section 6.1). For all sources, measured and simulated profiles were averaged in the axial direction over the 35 planes. To further improve signal/noise ratio, simulated data were averaged every four angular profiles, thus obtaining 84 angular views (resulting in an angular sampling of ≈2°). The scatter correction method, including a normalization procedure to scale the Monte Carlo simulated scatter distributions to the measured profiles, is described below and shown step by step in Fig.8 for the 8cm cylindrical source. In this procedure, to account for the smaller number of simulated angular profiles, four adjacent measured profiles were corrected with the same simulated scatter profile:

- filtering of the measured profiles, to smooth noise fluctuations (Fig.8a)
- definition of the edges of the source object as the points in the profiles characterized by the maximum slope (maximum absolute value of the angular coefficient of the straight line tangential to the profile) (Fig.8a)
- pixel by pixel calculation of the ratios between measured and simulated profiles externally to the defined object edges
- calculation of the scaling factors (one per profile) as the mean value of the ratios defined above
- normalization of the simulated profiles to the measured profiles (Fig.8b)
- subtraction of the normalized simulated profiles from the measured profiles (Fig.8c)

Results

Fig.9 and 10 show the measured (true+scatter) sinograms (top left), the simulated scatter sinograms (top right), the scatter corrected sinograms (bottom left), a selected profile (at 0°) from the scatter corrected sinogram (bottom right), as examples, for the 20cm cylinder and the 8cm off centered line source respectively. Scatter fractions calculated as the ratio of MC simulated scatter component (after normalization) and total measured events, averaged over the angular profiles, are reported in Table 4 for all sources considered. These values are consistent with scatter fraction values measured according to standard procedures (Table 3). This preliminary results indicate that the MC simulator combined with the normalization procedure properly models scatter component and can be used for scatter correction.

	cylinder A	cylinder B	line at 0cm	line at 4cm	line at 8cm
scatter fraction (%) corrected by MC	40.8	24.5	42.5	42.0	39.7

Table 5

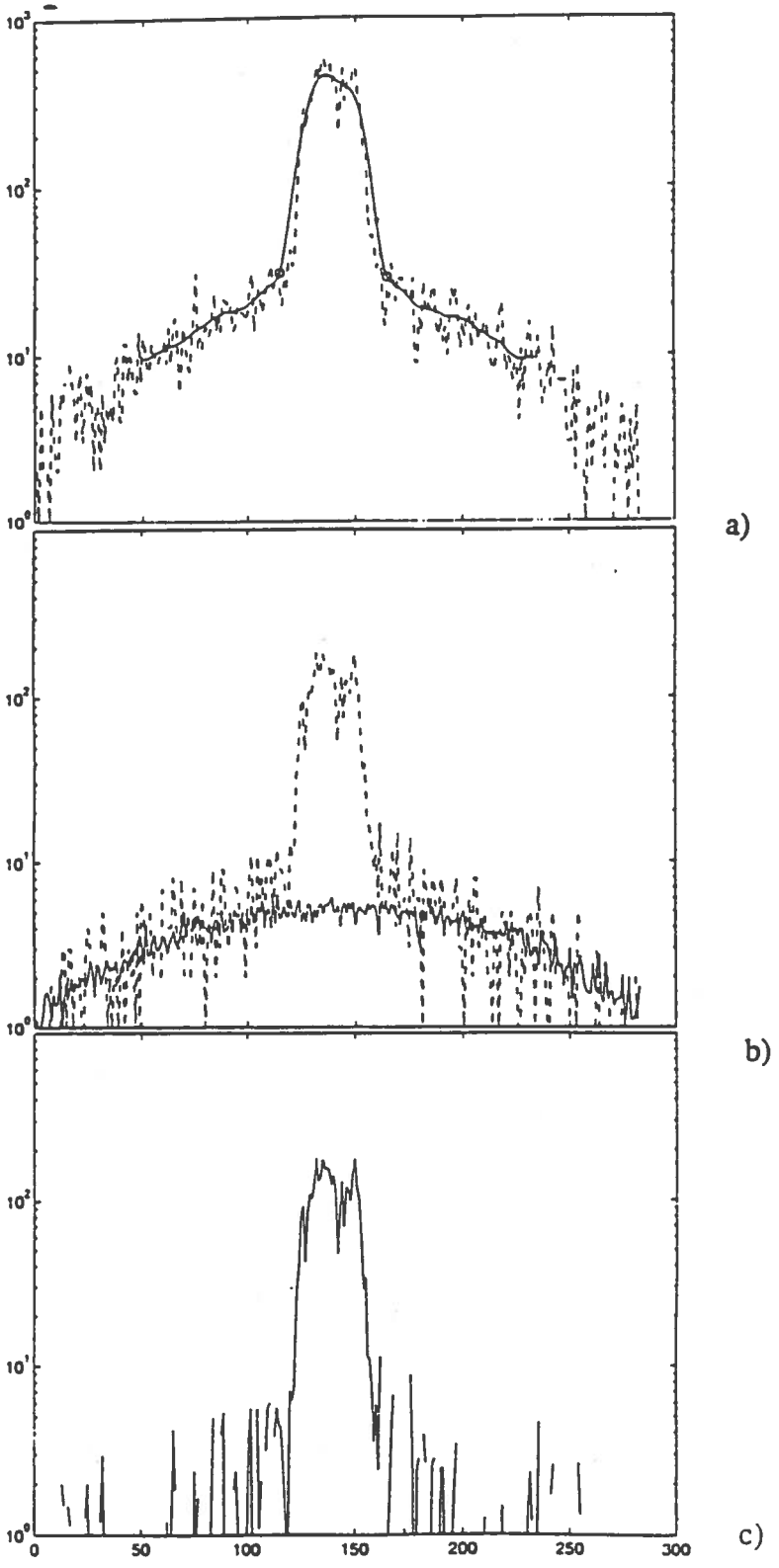

Fig. 8

Monte Carlo scatter correction method :

a) filtered measured profile (-) overlapped to the measured profile (--)

b) normalized simulated profile (-) overlapped to the measured profile (--)

c) corrected profile

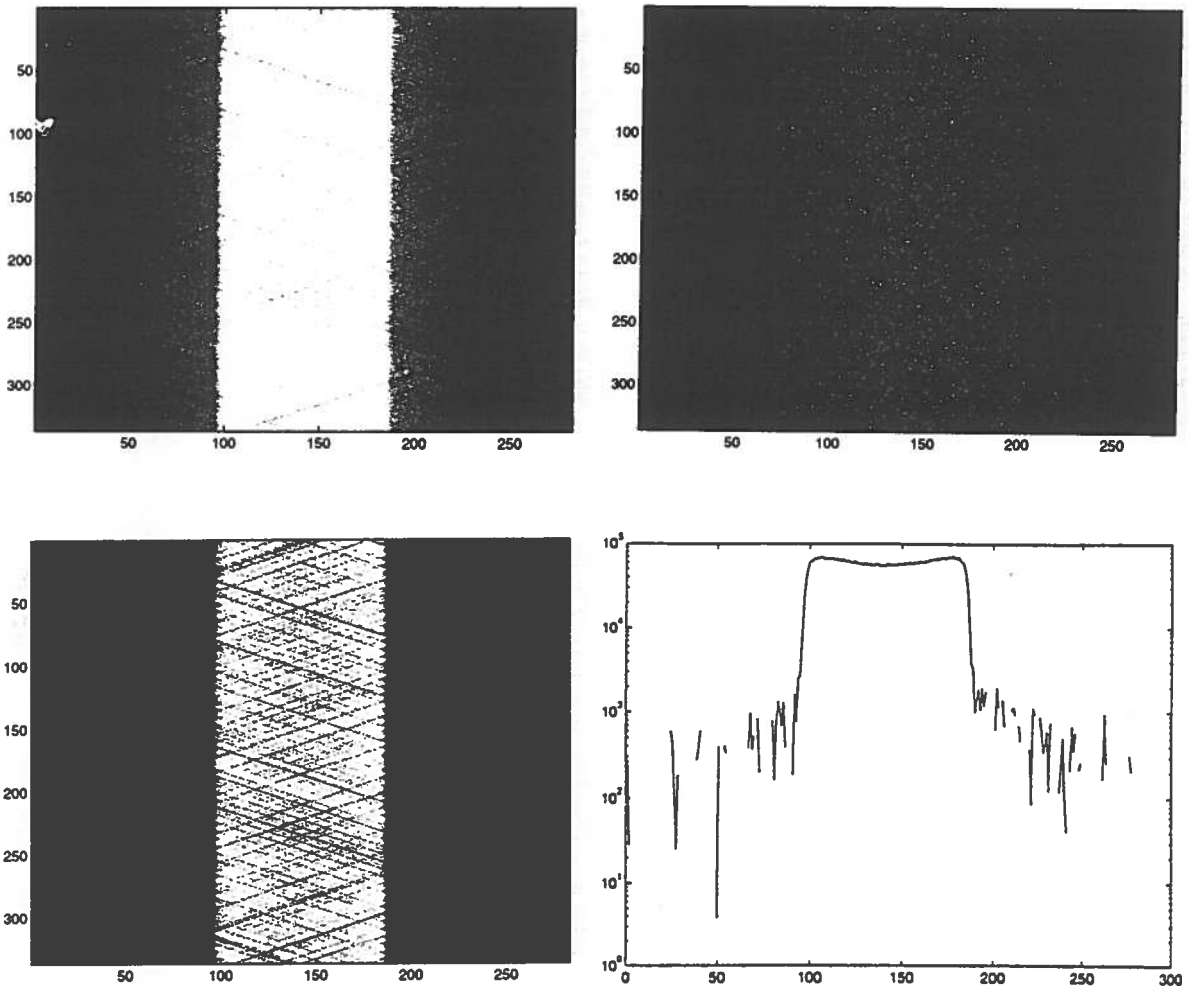

Fig. 9

Measured (trus+scatter) sinogram (top left), simulated scatter sinogram (top rigth), scatter corrected sinogram (bottom left), profile of the scatter corrected sinogram (bottom right) for the 20cm cylinder.

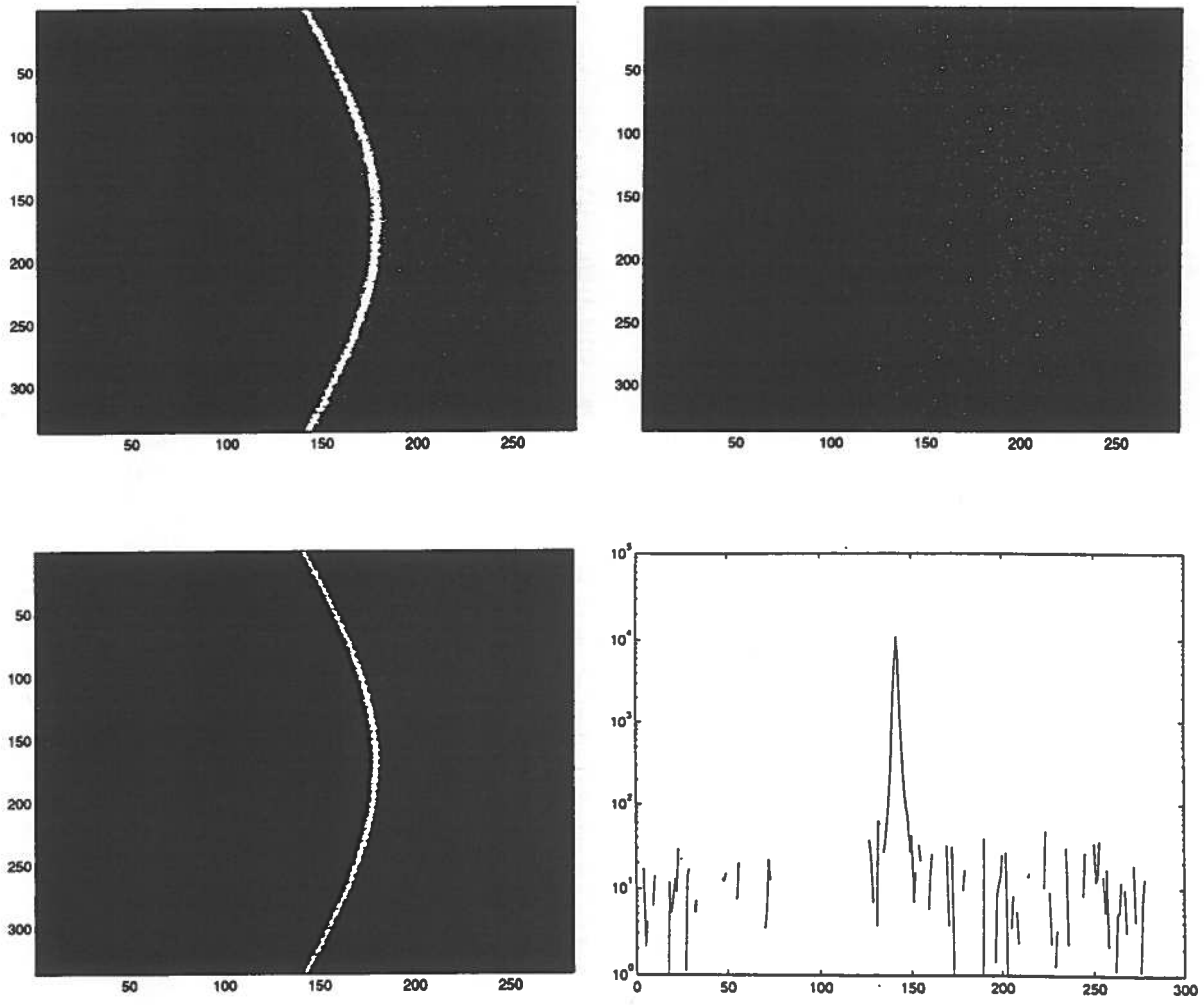

Fig. 10

Measured (trus+scatter) sinogram (top left), simulated scatter sinogram (top rigth), scatter corrected sinogram (bottom left), profile of the scatter corrected sinogram (bottom right) for the 8cm off centered line source.

7. - CONCLUSIONS

In this study, a MC package to simulate a current generation 3D PET scanner and radioactive sources was developed. The MC simulator was modeled to the Advance PET scanner, installed at Institute H S.Raffaele in Milan. The validity of the simulations was assessed by comparison with measured experimental data in the case of simple geometrical sources.

The MC program was then used focussing on the study of scattered radiations, the need for scatter correction representing a crucial issue in 3D PET. Scatter correction techniques require scatter distribution to be modeled and subtracted from measured data. Taking advantage of the ability of the MC method in yielding independent distributions of scattered and unscattered radiations for known radioactive sources, two approaches to scatter correction were investigated. An analytical technique fitting scatter component with a gaussian function was considered and the accuracy of such modeling was evaluated by statistical analysis. The feasibility of a MC based technique, modeling scatter distribution by a probabilistic approach, was also assessed.

This study represents the preliminary step for future investigations:

1. Further simulations with a higher number of generated events are required for the evaluation of the accuracy of the analytical gaussian fitting method, to reduce noise in the simulated data and allow more conclusive statistical tests.

2. In order to evaluate the clinical feasibility of the scatter correction analytical method, more complex source objects, better representing anatomical structures in the human body, require to be simulated. Analytical geometric functions are not adequate to describe such complex structures. Description of the source objects in terms of image matrices are then necessary, as could be provided by experimental clinical PET studies. The use of image matrices as source objects for MC simulations implies the need for software optimization to allow handling of source image matrices and reduction of computation times.

To note, the PET images representing the input source for the MC simulation of scatter distribution should be free from scatter contribution. PET images obtained in the 2D configuration could be employed. The low scatter component ($\approx$10%) characteristic of the 2D acquisition mode could be either corrected or accounted for in the interpretation of the results.

3. The use of the MC based scatter correction method should be extended to clinical studies, using clinical PET images as input sources for simulation. As proposed for the assessment of the clinical feasibility of the analytical scatter correction method, 2D PET studies could be assumed. However, a scatter correction method feasible for clinical applications requires a simple and fast acquisition protocol. Performing two PET studies, one in 3D configuration for the assessment of the radioactiviy distribution and one in 2D representing the input source for the MC based scatter correction method would not be compatible with this criterion. The straight use of 3D PET images would then be desirable, but in this case the input distribution of radioactivity concentration is overestimated as a result of the significant scatter

component. The effect of this approximation in modeling scatter distribution has to be evaluated.

In conclusion, the detection of scattered radiation is one of the major sources of artefact in 3D PET and scatter correction is mandatory for accurate quantification of PET data. MC simulation represents a powerful tool for modeling scatter component underlying the PET measured radioactivity distribution. The findings of the present work drive towards an extensive use of the developed MC program (PET-EGS) for the optimization and validation of scatter correction methods in 3D PET.

REFERENCES

1. J.E. Hoffman, M.E. Phelps, *Positron Emission Tomography: Principles and Quantitation*, Mazziotta and Schelber, Raven Press, New York 1986.
2. D.W. Townsend et al., IEEE Trans. Nucl. Sci., vol.36, pp.1056-1065, 1989, *Three Dimensional Reconstruction of PETDdata from a Ring Camera.*
3. C.J. Thompson, IEEE Trans. Med. Imag., vol.12, n.1, pp.124-132, 1993, *The Problem of Scatter Correction in Positron Volume Imaging.*
4. S.R. Cherry, M. Dahlbom and J.E. Hoffman, J. Comput. Assist. Tomogr., vol.15, n.4, pp.655-668, 1991, *3D PET Using a Conventional Multislice Tomograph without Septa.*
5. S.R. Cherry and S.C. Huang, IEEE Trans. Nucl. Sci., vol.42, n.4, pp.1174-1179, 1995, *Effects of Scatter on Model Parameter Estimates in 3D PET Studies of the Human Brain.*
6. M. Dahlbom et al., IEEE Trans. Nucl. Sci., vol.36, n.1, pp.1066-1071, 1989, *A Study of the Possibility of Using Multi-slice PET System for 3D Imaging.*
7. J.M. Ollinger, IEEE Trans. Nucl. Sci., vol.42, n.4, pp.1168-1173, 1995, *Detector Efficiency and Compton Scatter in Fully 3D PET.*
8. J.G. Rogers et al., IEEE Trans. Nucl. Sci., vol.39, n.4, pp.1063-1067, 1992, *An Improved Multicrystal BGO Detector for PET.*
9. M.P. Tornai, G. Germano and E.J. Hoffman, IEEE Trans. Nucl. Sci., vol.41, n.4, pp.1458-1463, 1994, *Position and Energy Response of PET Block Detectors with Different Light Sharing Schemes.*
10. D.L. Bailey and S.R. Meikle, Phys. Med. Biol., vol.39, n.5, pp.411-424, 1994, *A Convolution-Subctraction Scatter Correction Method for 3D PET.*
11. M. Bentourkia et al., J. Nucl. Med., vol.36, pp.121-130, 1995, *Assessment of Scatter Components in High-Resolution PET: Correction by Nonstationary Convolution Subtraction.*
12. S.R. Cherry, S. Meikle and E.J. Hoffman, J. Nucl. Med., vol.34, n.4, pp.671-678, 1993 *Correction and Characterization of Scattered Events in Three-Dimensional PET Using Scanners with Retractable Septa.*
13. J. Barney, R. Harrop and C. Dykstra, IEEE Trans. Nucl. Sci., vol.40, pp.1001-1007, 1993, *Source Distribution Dependent Scatter Correction for PVI.*

14. J. Ollinger and G. Jones, IEEE Nucl. Sci. Symp. and Med. Imag. Conf., San Francisco CA., pp.1264-1268, 1993, *Model-based Scatter Correction for Fully 3D PET.*
15. S. Grootoonk et al., IEEE Nucl. Sci. Symp. and Med. Imag. Conf., Orlando FL., pp.942-944, 1992, *Practical Implementation and Accuracy of Dual Window Scatter Correction in a NeuroPET Scanner with the Septa Retracted.*
16. D. Acchiappati, N. Cerullo and R. Guzzardi, Eur. J. Nucl. Med., vol.15, n.11, pp.683-686, 1989, *Assessment of the Scatter Fraction Evaluation Methodology Using Monte Carlo Simulation Techniques.*
17. P. Bertzakos and C.J. Thomson, IEEE Trans. Nucl. Sci., vol.38, n.2, pp.732-735, 1991, *A Depth-Encoded Pet Detector.*
18. J. Logan and H.J. Bernstein, J. Comput. Assist. Tomogr., vol.7, n.2, pp.316-320, 1983, *A Monte Carlo Simulation of Compton Scattering in Positron Emission Tomography.*
19. C. Michel et al., IEEE Trans. Med. Imag., vol.10, n.3, pp.240-248, 1991, *Assessment of Response Function in two PET Scanners with and without Interplane Septa.*
20. C. Moisan et al., IEEE Trans. Nucl. Sci., vol.43, n.3, pp.1974-1980, 1996, *A Monte Carlo Study of the Acceptance to Scattered Events in a Depth Encoding PET Camera.*
21. J.Nuyts, H.Bosmans and P.Suetens, IEEE Trans. Med. Imag., vol.12, n.3, pp.421-429, 1993, *An Analytical Model for Compton Scatter in a Homogeneusly Attenuating Medium.*
22. J.G. Rogers e al., IEEE Trans. Nucl. Sci., vol.36, n.1, pp.993-997, 1989, *Design of a Volume Imaging Positron Emission Tomograph.*
23. C.W. Stearns et al., IEEE Trans. Nucl. Sci., vol.35, n.1, pp.708-711, 1988, *Simulation Studies for Cylindrical Positron Tomography.*
24. N.A. Keller and L.R. Lupton, IEEE Trans. Nucl. Sci., vol.NS-30, n.1, pp.676-680, 1983, *PET Detector Ring Aperture Function Calculations Using Monte Carlo Techniques.*
25. H. Zaidi and C. Morel, Internal Report, 1995, *Design and Implementation of an Object-Oriented Sofware Tool for Monte Carlo Simulation of 3D PET Scanners.*
26. R.L. Harrison et al., IEEE Nucl. Sci. Symp. and Med. Imag. Conf., San Francisco CA., pp.1154-1158, 1993, *Preliminary Experience with the Photon History Generator Module of a Public-Domain Simulation System for Emission Tomography.*
27. R.A. Brooks and G. Di Chiro, Phys. Med. Biol., vol.21, n.5, pp.689-732, 1976, *Principles of Computer Assisted Tomography (CAT) in Radiographic and Radioisotopic Imaging.*
28. T.R. DeGrado et al., J. Nucl. Med., vol.35, pp.1398-1406, 1994, *Performance Characteristics of a Whole-Body PET Scanner.*
29. K. Wienhard et al., J. Comput. Assist. Tomogr., vol.16, pp.804-813, 1992, *Performance Evaluation of the Positron Scanner ECAT EXACT.*
30. T.J. Spinks et al., Phys. Med. Biol., vol.37, n.8, pp.1637-1665, 1992, *Physical Performance of a Positron Tomograph for Brain Imaging with Retractable Septa.*
31. D.W. Townsend et al., J. Nucl. Med., vol.34, n.8, pp.1367-1376, 1993, *A Rotating PET Scanner using BGO Block Detectors: Design, Performance and Applications.*

32. K. Wienhard et al., J. Comput. Assist. Tomogr., vol.18, n.1, pp.110-118, 1994, *The ECAT EXACT HR: Performance of a New High Resolution Positron Scanner.*
33. T.K. Lewellen et al., IEEE Trans. Nucl. Sci., vol.43, n.4, pp.2199-2206, 1993, *Investigation of the Performance of the General Electric Advance Positron Emission Tomograph in 3D Mode.*
34. C.W. Stearns, S.R. Cherry and C.J. Thompson, IEEE Trans. Nucl. Sci., vol.42, n.4, pp.1075-1079, 1995, *NECR Analysis of 3D Brain PET Scanner Designs.*
35. D.L. Bailey et al., IEEE Trans. Med. Imag., vol.10, n.3, pp.256-260, *Noise Equivalent Count Measurements in a Neuro-PET Scanner with Retractable Septa.*
36. T.K. Lewellen et al., IEEE Trans. Nucl. Sci., vol.42, n.4, pp.1051-1057, 1995, *Investigation of the Count Rate Performance of General Electric Advance Positron Emission Tomograph.*
37. C.W. Stearns and D.C. Wack, IEEE Trans. Med. Imag., vol.12, n.2, pp.287-292, 1993, *A Noise Equivalent Counts Approch to Transmission Imaging and Source Design.*
38. C.J. Thompson, IEEE Trans. Nucl. Sci., vol.36, n.1, pp.1072-1077, 1989, *The Effect of Collimation on Singles Rates in Multi-Slice PET .*
39. M. Dahlbom et al., IEEE Trans. Nucl. Sci., vol.40, n.4, pp.1048-1054, 1993, *Optimization of PET Instrumentation for Brain Activation Studies.*
40. R. Myers et al., NeouroImage, vol.5, n.4, b15, 1997, *The Use of 2D and 3D PET and [11C]R-PK11195 to Image Focal and Regional Brain Pathology.*
41. H.O. Anger, J. Nucl. Med., vol.5, pp.515-531, 1964, *Scintillation Camera with Multichannel Collimators.*
42. M. Defrise, A. Greissbuhler and D.W. Townsend, Phys. Med. Biol., vol.39, n.3, pp.305-320, 1994, *A Performance Study of 3D Reconstruction Algorithms for Positron Emission Tomography.*
43. D.W. Townsend et al., IEEE Trans. Med. Imag., vol.10, pp.505-512, 1991, *Fully Three Dimensional Reconstruction for a PET Camera with Retractable Septa.*
44. A.F. Bielajew, Report PIRS-0393, Institute for National Measurement Standards, National Research Council of Canada, Ottawa, Canada, *Photon Monte Carlo Simulation.*
45. G.F. Knoll, *Radiation Detection and Measurement*, J.Wiley & Sons, 1979.
46. *General Electric Internal Report*, enclosed document with PET Advance manuals.
47. J.S. Karp et al., J. Nucl. Med., vol.32, pp.2342-2350, 1991, *Performance Standards in Positron Emission Tomography.*
48. M. Bentourkia et al., IEEE Trans. Nucl. Sci., vol.42, n.4, pp.1162-1167, 1995, *Object and Detector Scatter Function Dependence on Energy and Position in High Resolution PET.*
49. J.S. Karp et al., J. Nucl. Med., vol.31, pp.617-627, 1990, *Continuous-Slice-PENN-PET: A Positron Tomograph with Volume Imaging Capability.*
50. C.S. Levin, M. Dahlbom, E.J. Hoffman, IEEE Trans. Nucl. Sci., vol.42, n.4, pp.1181-1185, 1995, *A Monte Carlo Correction for the Effect of Compton Scattering in 3D PET Brain Imaging.*